

Experimental investigation of vortex ring evolution in polymer solution

Swastik Hegde, Shashank H J, and K R Sreenivas

Engineering Mechanics Unit, Jawaharlal Nehru Centre for

Advanced Scientific Research, Bangalore 560064, India

(Dated: February 1, 2022)

Abstract

We have conducted experiments on the effect of polymer solutions on the formation and propagation of vortex rings. We study this effect in aqueous solution of hydrolyzed polyacrylamide (PAMH) at different concentrations. Addition of PAMH imparts shear-rate dependent viscosity and elasticity to the solvent. With increasing concentration of PAMH both the zero-shear-rate viscosity (η_0) and the infinite-shear-rate viscosity (η_∞) increase. The relaxation time also increase with the increase in concentration. We generate vortex rings using a piston-cylinder mechanism in a glass tank and measure vortex ring properties such as ring position, ring circulation, enstrophy, kinetic energy and peak vorticity using particle image velocimetry (PIV). Experiments are conducted by (1) matching impulse, and (2) matching Reynolds number. We show that, at constant impulse, vortex ring properties in PAMH solution deviate from that in Newtonian water. As the concentration of the PAMH solution increases, so too does the deviation from water. We further perform experiments in water by matching the limiting Reynolds numbers of the PAMH solution corresponding to both η_0 and η_∞ . We find that while the circulation of PAMH solutions lie between the circulation curves of the two extreme Reynolds number matched water experiments for an extended period of time, the enstrophy and peak vorticity do not. We attribute this behaviour to the modification of vorticity distribution within the core of vortex rings in PAMH solutions. We also study the effect of polymer solutions on the formation number. We find that the formation number remains the same even in polymer solutions. We also demonstrate, using planar laser induced fluorescence (PLIF), the phenomenon of ring reversal. Once the vortex ring stops, it begins to unwind and retract by translating and rotating in the opposite direction. We attribute this behaviour of ring reversal to the elastic properties of polymer solutions.

I. INTRODUCTION

Vortex rings are self-driven coherent structures and vortices are ubiquities in turbulent flows. Vortex rings are studied extensively for their rich physics and their relevance in various flow contexts. Their interaction with density interface is relevant in understanding the mixing process [1, 2], vortex-breakdown for understanding the transition to turbulence, quantum turbulence [3] and entrainment process in turbulent jets and plumes [4, 5]. Interaction of vortices and their dynamics plays an important role in energy cascade in turbulent flows. Gharib et. al. [6] have proposed a method to measure cardiac health by determining the strength of vortex rings formed as blood passes through the valves within the heart, and recently it has been shown that vortex rings can be used for cell encapsulation [7]. These biological fluids are known to exhibit non-Newtonian behavior, as do fluids in many industrial flows. The study of vortex rings in non-Newtonian fluids is thus very relevant. However, there are only a few detailed studies on vortex rings in non-Newtonian fluids.

Palacios-Morales and Roberto Zenit [8] have studied the behaviour of the vortex ring in shear-thinning liquids at low Reynolds number. The shear-thinning fluids have been characterized using the power-law model. The Reynolds number of the shear-thinning vortex ring was calculated using a characteristic shear rate, and the ring thus generated was compared with a Newtonian vortex ring at the same Reynolds number. They find that the shear-thinning fluid retards the vortex ring, leading to a reduction in its propagation properties. Bentata et al. [9] studied vortex rings in shear-thinning solutions at low Reynolds number ($Re \approx 30$ to 300). Their findings of the propagation properties of the vortex ring, for instance the ring velocity and ring diameter are in agreement with that obtained by Palacios [8]. In another study, Palacios-Morales et. al. [10] studied the effect of viscoelasticity on vortex rings at low Re . The vortex ring showed a reduction in its circulation at the end of the formation stage. Formation of a ‘negative’ vortex ring ahead of the primary ring was also observed.

A shear-thinning fluid typically exhibits viscosity plateaus at both zero-shear-rate (η_0) and infinite-shear-rate (η_∞). The Carreau-Yasuda model, which captures these plateaus, is thus better suited for characterization of these polymer solutions than the power-law model

[11]. Depending on the shear rates, vortex ring can experience two distinctive viscosity variation, (1) power-law variation, and (2) a constant viscosity corresponding to the viscosity plateaus. The reduction in the shear rate as the ring propagates forward leads to an increase in the local viscosity, which further retards the ring. Crucially, at low Re (as seen in the experiments of Palacios-Morales [8] and Bentata et. al. [9]), the shear rates experienced by the ring is at the low shear rate end of power-law region, and quickly enter into the zero shear plateau as the ring propagates forward. Additionally, in the aforementioned studies, the viscosity of the non-Newtonian fluids is significantly larger than the water viscosity.

We study vortex rings in non-Newtonian polymer solutions at large Reynolds numbers. We choose polymer solution viscosities that are akin to those used in polymer drag reduction applications. The shear viscosity of the non-Newtonian fluids in this study are of the order of magnitude of Newtonian water. PAMH solutions used in this work are shear thinning, and are characterized using the Carreau-Yasuda model. The shear rates corresponding to the Reynolds numbers considered are closer to the infinite-shear-rate plateau. Thus the vortex ring experiences the whole power-law region and the zero shear plateau, as opposed to the shear rates observed in literature. This study of the canonical form of vorticity in the presence of polymer solutions helps in building toy models to shed light on the mechanism of the complex phenomenon of turbulent polymer drag reduction.

In this paper, we experimentally compare vortex ring formation and its free-shear motion in PAMH polymer solution with that in water. Key quantities of vortex-ring evolution, such as circulation, enstrophy, kinetic energy and peak vorticity are measured using PIV. We report the key difference regarding vorticity distribution in two scenarios observed in our experiments. We also demonstrate that the Reynolds number matching alone for vortex rings in two different solutions would not account for their behaviour. We also show that formation number is independent of the fluid properties used in the current experiments.

II. EXPERIMENTS

We generate vortex rings using a piston-cylinder mechanism driven by a servomotor, with control over the piston speed (V) and the piston stroke length (L). The servomotor operates

on a closed-loop servo system, with an optical encoder. We generate the vortex rings in a glass tank ($3\text{ m} \times 0.75\text{ m} \times 0.75\text{ m}$) with a capacity of ≈ 1500 litres. A nozzle with exit diameter (D) of 50 mm is connected at the end of the piston-cylinder arrangement. The exit of the nozzle is located at a distance of 300 mm ($6D$) from both the bottom of the tank and the free surface of the fluid. The exit of the nozzle is 300 mm from the end of the back wall of the tank and 300 mm from the side walls of the tank. The walls of the tank are sufficiently far away from the nozzle to make end effects negligible. A schematic of the experimental arrangement is shown in Fig. 1.

We perform 2-D particle image velocimetry (PIV) and planar laser induced fluorescence (PLIF) to study the vortex rings. A vertical laser sheet is generated from one end of the tank to the other using a combination of spherical and cylindrical lenses. We utilise a Litron (nano-series) pulsed, dual-head Nd-YAG laser, with a wavelength of 532 nm . The lasers are operated at an intensity of 100 mJ per pulse with a repetition rate of 25 Hz . The time delay between the two laser heads is controlled using a Stanford delay generator. We utilise a Phantom Speedsense 9040 high speed camera with a resolution of 2 megapixels to acquire the image maps. The camera is synchronized with the laser using the same Stanford delay generator. We use a ΔT of 1 ms between the two laser heads to ensure that the strong vortical regions of the vortex rings are adequately captured. These strong vortical regions require a good concentration of seeding particles to obtain good correlations in the PIV analysis. We add 1 g of seeding particles (polyamide particles of size $50\text{ }\mu\text{m}$ and density 1.2 g/cm^3) exclusively to vortex rings over the trials, in addition to 2 g of seeding particles that are added to the whole tank. The PIV analysis is performed using an interrogation window of $32\text{ pixels} \times 32\text{ pixels}$ with an overlap of 50%. Further information about PIV can be found in [12–16]. Our PIV analysis yields a 2-D velocity field, with radial and axial components of velocities. Additional details of the experimental arrangement can be found in [17].

In this work, we extract the properties of vortex ring as it propels forward due to self-induced velocity. We calculate the peak azimuthal ring vorticity, enstrophy, kinetic energy, circulation and ring position. We evaluate the azimuthal vorticity by taking a curl of the 2-D velocity vectors. We calculate the enstrophy and kinetic energy over the whole field. The ring circulation is evaluated over one half of the ring. Finally, we evaluate the ring

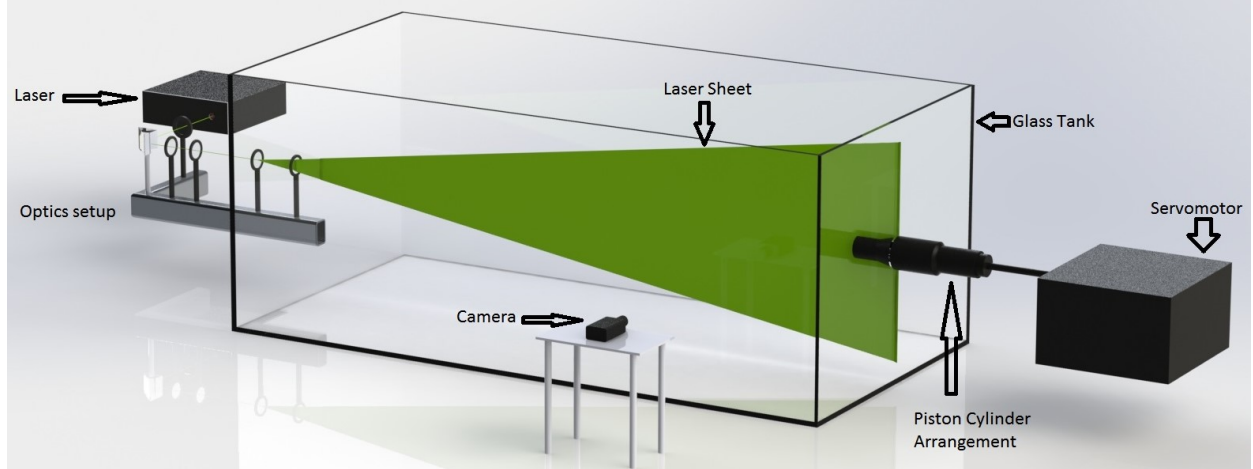


FIG. 1. Schematic of experimental setup

position by finding the locations corresponding to the peak azimuthal vorticities within the ring.

We study the effect of polymer solutions on vortex rings by performing four types of experiments: (1) matched impulse experiments (Section IV), (2) matched Re (Section V) experiments, (3) formation number (L/D) experiments (Section VI), and (4) vortex ring reversal (Section VII). For (1) and (2), the piston stroke-length L is kept constant at 100 mm , and piston velocity V is varied. With this arrangement, we generate vortex rings over a large range of Re (1000 to 100000). The Reynolds number for the current experiments is calculated based on the piston input parameters - $Re = LV/\nu$. For (3), the piston velocity V is maintained constant at 500 mm/s , while the stroke length L is varied to obtain different values of L/D . For (4), PLIF is performed at low values of Re . The nomenclature used in this paper is $L_{xxx} V_{yyy}$, where xxx and yyy corresponds to the stroke length L and piston velocity V , respectively. For instance, $L_{100} V_{500}$ corresponds to an experiment with a stroke length L of 100 mm and a piston velocity V of 500 mm/s .

The polymer solution is prepared in de-ionised (DI) water with a resistivity of 4 $M\Omega m$. The required quantity of polymer is mixed in a container (of about one-tenth the volume of the tank) using a mechanical stirrer, yielding a thickened solution. This thickened solution is then diluted to the required concentration by slowly mixing it with de-ionised water in the glass tank. The solution in the tank is allowed to homogenize for 48 hours, after which

the experiments are conducted.

III. POLYMER SOLUTION CHARACTERIZATION

We use hydrolyzed polyacrylamide (PAMH) as the polymer in our experiments. The polymer has a molecular weight $12-16 \times 10^6$. We prepare three different polymer solutions with concentrations of 5 *ppm*, 10 *ppm* and 25 *ppm*. In this section, we measure the rheological properties of these polymer solutions. The shear thinning property of polymer solutions is characterized using the Carreau-Yasuda model. The rheological properties of interest are the zero-shear viscosity η_0 , the infinite-shear viscosity η_∞ , the power-law index n , and relaxation time λ . The first three parameters characterize shear-thinning behaviour, while the relaxation time characterizes the elasticity of the solution.

Fig. 2 shows the shear-thinning viscosity profile measured using rotational rheometry. We use an Anton-Paar MCR 302 rheometer with a double gap geometry to perform these measurements. We see from the plots that, as the shear rate increases, polymers gets stretched and aligned along the flow direction. This leads to a reduced resistance to the flow, thereby leading to a reduced viscosity at high shear-rates. We see from the plots that, the viscosities of the polymer solution increases with the increase in the polymer concentration. This is apparent from the viscosity plots shown for three polymer solutions in Fig. 2a (PAMH 5 *ppm*), Fig. 2b (PAMH 10 *ppm*) and Fig. 2c (PAMH 25 *ppm*). All the rheological properties obtained from Carreau-Yasuda model are shown in Table I.

In our experiments, the shear rate of the shear layer pushed out of the piston, which rolls up to form the vortex ring is $\mathcal{O}(100)$ 1/*s*. This means that, during the formation stage of the vortex ring, the viscosity in the shear layer is $\approx \eta_\infty$ (see Fig. 2). As the vortex ring propagates, the slow reduction in its velocity due to viscous effects causes an increase in the viscosity. This increase in viscosity will reduce the ring velocity further, which leads to a further increase in viscosity, and so on. This process continues till the zero shear plateau is reached, at which the viscosity is η_0 . Therefore, the viscosities experienced by the vortex ring vary from η_∞ to η_0 through the power law region. However, the ambient, being station-

ary, is always at η_0 . The effects of shear thinning are thus significant, and cannot be ignored.

We tried to measure the elasticity through oscillatory rheometry using various techniques. However, both storage and loss modulus were very small for the direct measurement. However, in Carreau-Yasuda model, inverse of the shear rate at which the transition from zero-shear plateau to power law region occurs, is a measure of the relaxation time [18, 19]. Hence, we obtain the relaxation time from the shear-thinning viscosity profile by using the Carreau-Yasuda model.

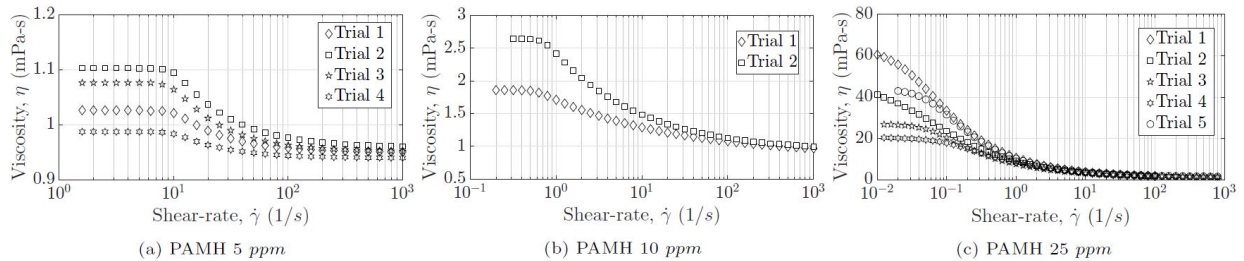


FIG. 2. Viscosity vs. shear rate for the PAMH solutions

Solution	λ (s)	n	η_0 (mPa-s)	η_∞ (mPa-s)
PAMH 5 ppm	0.1	–	1.0 - 1.1	0.95
PAMH 10 ppm	1 - 2	0.58 - 0.68	2 - 3	0.955
PAMH 25 ppm	12 - 25	0.46 - 0.56	20 - 60	0.96

TABLE I. Carreau-Yasuda parameters for the PAMH solutions

IV. VORTEX RINGS AT MATCHED IMPULSE

In this section, we present experiments on vortex rings in water and in PAMH solutions at the same impulse. Vortex ring experiments where initial impulse provided for polymer solution is same as its Newtonian counterpart is the simplest and rudimentary way to examine the effect of polymers. Experiments at matched impulse can be considered as an analog for certain commercial situations, such as pipeline and pumping network, where the power input has already been fixed. The impulse is matched by maintaining the same piston

parameters, i.e., the stroke length and piston velocity across the different fluids. The piston impulse range is divided into three categories: (1) low impulse - L100 V100, (2) medium impulse - L100 V500, and (3) high impulse - L100 V1000.

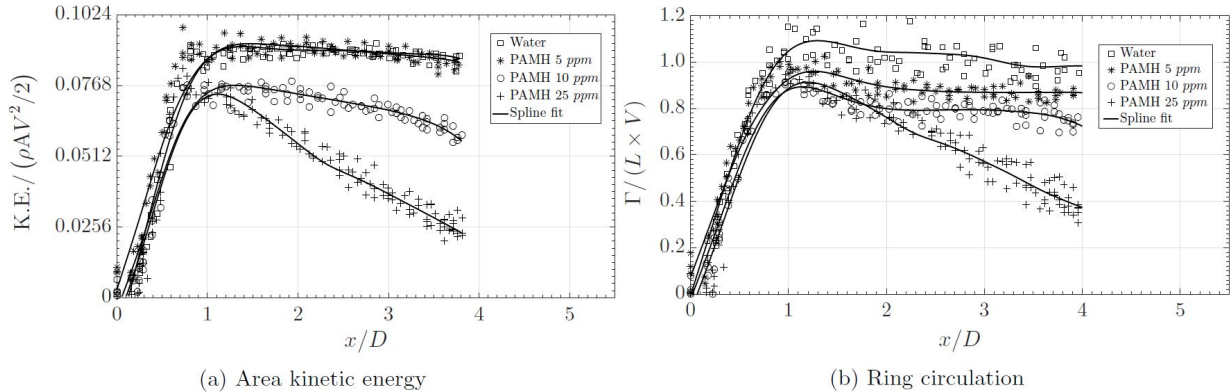


FIG. 3. Area kinetic energy and ring circulation for all fluids at L100 V500.

Fig. 3 shows the behaviour of the non-dimensional ring circulation and the non-dimensional area kinetic energy for all fluids at L100 V500. The evolution of ring circulation is shown in Fig. 3b. We see from the plots that the ring circulation increases for an initial duration of the flow. This corresponds to the formation stage of the vortex ring. This formation process occurs over an axial distance of $\approx 1D$. At the end of the formation stage, all four solutions have the same values of ring circulation. The circulation contained in the shear-layer feeding the vortex ring is thus conserved in all the four solutions. We also see from the plots that, for water, the ring circulation remains nearly a constant during the free shear motion of the vortex ring (after the formation stage ends). However, the polymer solutions show a reduction in ring circulation during free shear motion. Furthermore, the reduction in ring circulation is more drastic as the polymer concentration increases. This reduction in the ring circulation during free shear movement can be explained by the shear thinning viscosities of the polymer solutions. The propagating vortex ring is surrounded by ambient fluid which is at higher viscosity. The zero-shear viscosity η_0 of, say, the PAMH 25 ppm solution is 20-60 times the viscosity of water. Hence, the moving vortex ring experiences higher viscous dissipation at the edges, leading to a reduction in circulation. This reduction in circulation causes the ring to move slower, thereby reducing the shear rate within the ring, which aids further viscous dissipation due to the increase in viscosity. This

mechanism of viscous dissipation of circulation could also explain the degree of reduction of ring circulation of the PAMH 10 ppm and the PAMH 5 ppm solutions - the lower value of η_0 causes a lesser reduction in ring circulation. The area kinetic energy is the kinetic energy evaluated for the whole field, and is plotted in non-dimensional units in Fig. 3a. It is evident from the plot that, at the end of the formation stage, kinetic energy in the field is nearly the same for all the fluids. However, as the vortex ring propagates further downstream, we observe a reduction in the kinetic energy for PAMH 10 ppm and 25 ppm solutions. As explained for the ring circulation, this reduction in kinetic energy can also be attributed to the considerable increase in viscosity of these two solutions.

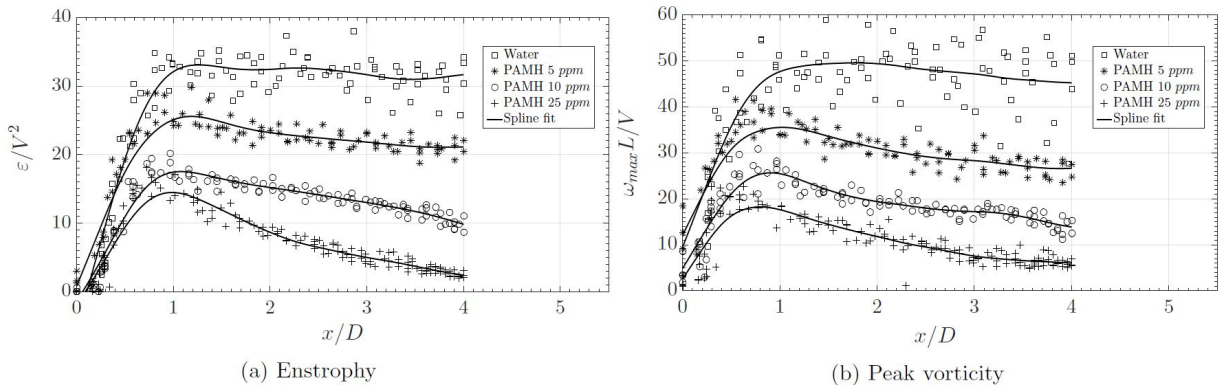


FIG. 4. Variation of enstrophy and peak vorticity of the vortex rings for all fluids at L100 V500

The variation of peak vorticity and enstrophy are plotted in Fig. 4. We see from the plots that, as the concentration of PAMH increases, the values of enstrophy and peak vorticity reduce during the initial formation stage of the ring. This is a clear difference from the behaviour of the circulation, which showed same values for the different polymer solutions during the formation stage. We present the vorticity distribution on one-half of the ring in Fig. 5 for water, PAMH 5 ppm and PAMH 10 ppm solutions. It is evident that the polymers in solution modify the vorticity distribution when the impulse is same. Water shows a narrow vorticity distribution with a higher peak, while the polymer solutions show a broader distribution with a lower peak. As the concentration increases, the vorticity distribution becomes flatter. We can now explain the behaviour of the ring circulation, area kinetic energy, enstrophy and peak vorticity as shown in Figs. 3 and 4: Shear rates in the shear-layer which feeds into vortex ring are $\mathcal{O}(100)1/s$. Hence, the viscosity encountered

by the shear-layer in all the polymer solutions is nearly the same i.e. η_∞ . Because of this, the vorticity (hence circulation) fed to the vortex ring through the shear-layer is conserved, across all the solutions. However, the shear-layer curls up in different manner to form the ring, thereby giving rise to different vorticity distribution in polymer vortex rings. This modification in vorticity distribution is such that, it gets broader with lower peak, as the polymer solution concentration increases. This broadening of the vortex ring core with lower peak values is the reason for reduced enstrophy and peak vorticity at the end of the formation stage.

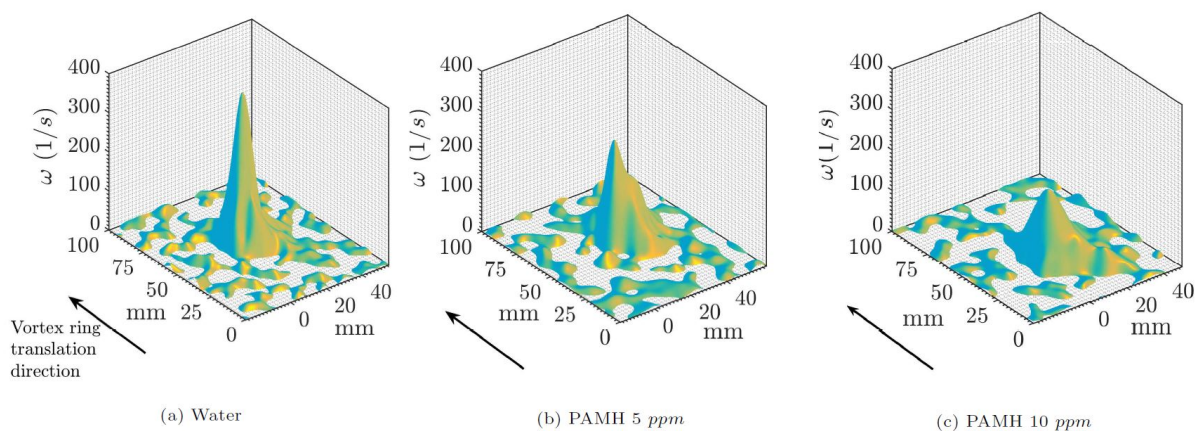


FIG. 5. Vorticity distribution over one-half of the vortex ring for Water, PAMH 5 ppm and PAMH 10 ppm at L100 V1000.

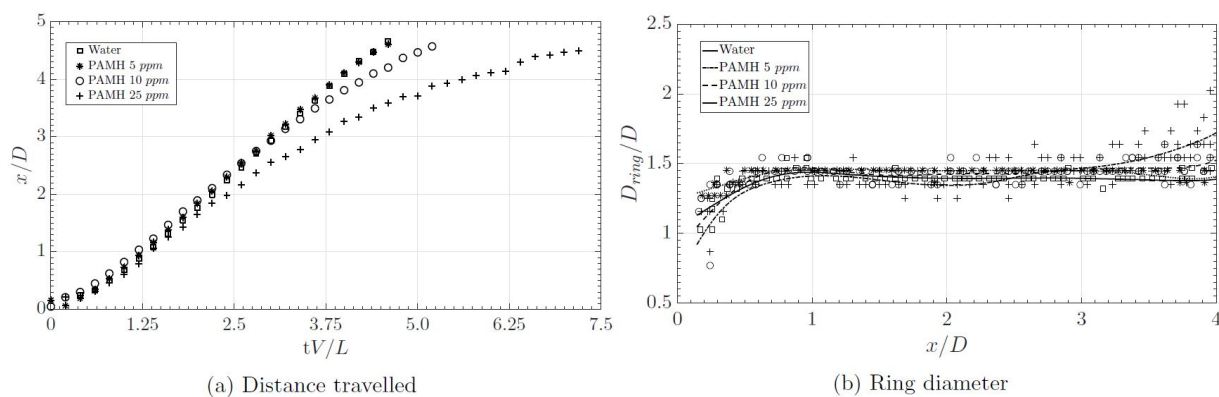


FIG. 6. Distance travelled by the vortex ring and ring diameter for all fluids at L100 V500.

Fig. 6 shows the distance travelled by the rings and the ring diameter in non-dimensional

units for all fluids at L100 V500. The distance travelled by the vortex ring is a function of translational velocity, which is in turn dependent on the ring circulation, ring diameter and core thickness. We observe that for the first $2D$ distance, vortex rings in all polymer solutions travel with same speed as that of water rings. We speculate that, for the initial distance, rings are driven by inertia of the fluid pushed by piston, rather than vortex ring's self induced velocity. After the first phase of inertia driven movement, vortex rings travel by their self induced velocity. We see, from the distance traveled plots (Fig. 6a), that the increase in concentration of the PAMH solution increases the deviation of the curve when compared to that of Water. The significant reduction in ring circulation for the PAMH 10 *ppm* and PAMH 25 *ppm* solutions during their free shear motion contribute to the deviation from Newtonian behaviour observed. The behaviour of the ring diameter is shown in Fig. 6b. The plot shows that, the ring diameter is unchanged in the presence of dissolved polymers in solution for the majority of the ring's motion. However, the PAMH 25 *ppm* solution shows an enhanced diameter beyond a distance of $3D$. This increase in diameter is also present in the PAMH 10 *ppm* solution, but to a lesser extent. The increase in ring diameter is associated with the reduction in circulation and translational velocity during the free shear motion of the ring.

We see from the experiments at matched impulse that the vorticity distribution of the vortex ring core is significantly altered by the polymer solutions, and this alteration leads to changes in the peak vorticity and enstrophy in the formation stage of the vortex ring. The circulation, kinetic energy, distance travelled and ring diameter show similar values during the formation stage, but begin to deviate from Newtonian behaviour during the free-shear motion of the ring. In a Newtonian fluid, the normalised vorticity distribution for propagating vortex rings at all times (or axial locations) are self-similar Gaussian profiles [20]. The polymer solutions clearly break this self-similarity, thereby causing the observed changes in the vortex ring properties. Furthermore, difference in vorticity distribution gets amplified as vortex rings traverse downstream, thereby showing increased deviation in the properties measured for the polymer solutions as compared to water. However, it has to be kept in mind that the Reynolds numbers of water vortex rings and the polymer vortex rings are not matched. Hence, to investigate the possible contribution of this Reynolds number mismatch to the above observations, we have carried out Reynolds number matched

experiments, which is explained in the following section.

V. VORTEX RINGS AT MATCHED REYNOLDS NUMBERS

The characteristics of a Newtonian vortex ring are a function of the L/D ratio, piston velocity history and the Reynolds number [21]. In theory, if these three parameters are matched for vortex rings in two different Newtonian solutions, then further evolution of those rings is same in non-dimensional co-ordinates. In the preceding section, we matched the L/D ratio and the piston velocity history for both Water and the polymer solutions. In this section, we perform experiments by matching the Reynolds numbers of the Water and PAMH vortex rings.

The Reynolds number ($Re = LV/\nu$) is to be matched by increasing L and/or V to compensate for the increase in ν . The PAMH solutions in this study show a shear-thinning behaviour with zero shear and infinite shear plateaus (see Fig. 2), which makes defining a single ν for the matching Re difficult. Multiple methods have been used to calculate the Reynolds number for vortex rings generated in a shear-thinning fluid. Olsthoorn et. al. [11] uses η_0 , the zero-shear viscosity, as the reference viscosity to calculate the Reynolds number. Palacios Morales [8] and Palacios Morales et. al. [10] calculate the Reynolds number for a shear thinning fluid using η of characteristic shear rate. Bentata et. al. [9] calculates a generalized Reynolds number, which is obtained by theoretically solving for the friction factor f as a function of Re for a shear thinning fluid in a laminar pipe flow.

In this study, we propose a method, which involves enveloping the whole Re range of polymer vortex rings, by considering two limiting Re , instead of matching a particular Re . We define two Reynolds numbers, at the extreme ends of the shear-thinning viscosity profile and conduct water experiments at those Reynolds numbers. By defining two limiting Reynolds numbers, we avoid any misrepresentation of the polymer solutions, since these Reynolds numbers signify the minimum ($Re_0 = VL/\nu_0$) and maximum ($Re_\infty = VL/\nu_\infty$) values attainable by the polymer solution vortex rings. The actual Reynolds number of the vortex ring in polymer solutions will always lie in between the two limiting values. We show

this graphically in Fig. 7. The plot shows the shear thinning viscosity profile for a typical polymer solution. The limiting Re values are indicated in the plot.

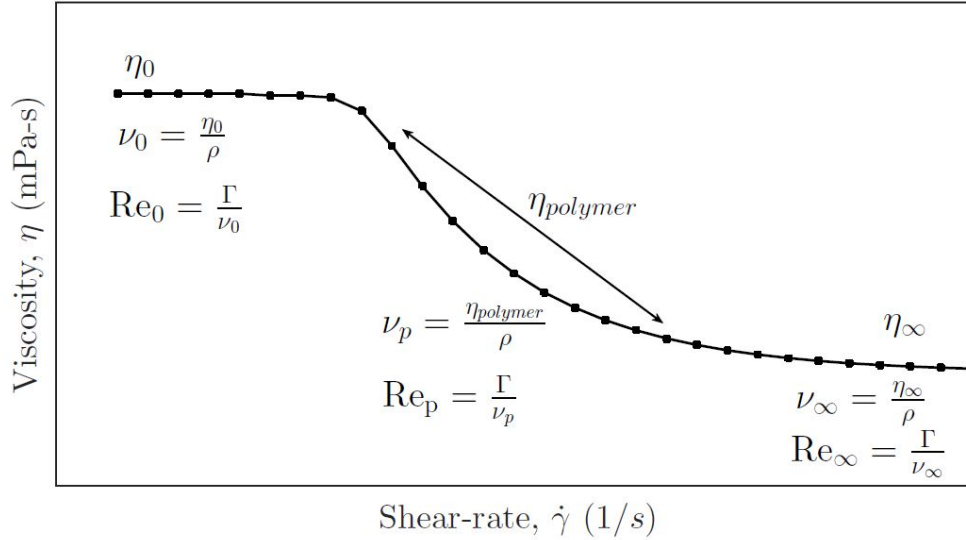


FIG. 7. Reynolds number defined for polymer solutions.

We perform vortex ring experiments at Re_0 and Re_∞ in water and compare the behaviour of these rings with that of the vortex rings in the polymer solution. We obtain different values in the Reynolds number by varying the circulation of the ring (Note: $\Gamma \sim L \times V$). Specifically, we vary the piston velocity V to vary the circulation and maintain the stroke length L at 100 mm for all the experiments. We keep the stroke length a constant in order to maintain constant values of L/D across all fluids. The values of η_0 and η_∞ that are obtained from the Carreau-Yasuda model, as shown in Table I, are used to calculate Re_0 and Re_∞ . These values of the limiting Reynolds numbers are shown in Table II along with all the other parameters of Re matched experiments. For example, the L100 V100 experiments of the PAMH 5 *ppm* solution will be compared with L100 V86 (corresponding to Re_0) and L100 V94 (corresponding to Re_∞) of water experiments. We present the experiments at matched Reynolds number for the PAMH 5 *ppm* and the PAMH 10 *ppm* solutions.

As shown in table II, L100 V100 experiment of PAMH 5ppm will be compared with L100 V86 and L100 V94 of water experiments. Similarly other experiments in polymer solutions are compared with their respective water counterparts.

Polymer solution	η_0 (mPa-s)	η_∞ (mPa-s)	In polymer solution	In water	
			V (mm/s)	V (To match Re_0) (mm/s)	V (To match Re_∞) (mm/s)
5ppm	1.05	0.95	100	86	94
			500	429	471
			1000	857	943
10ppm	2.25	0.955	100	40	94
			500	200	471
			1000	400	943
25ppm	40	0.96	500	11.25	471
			1000	22.50	943

TABLE II. Input parameters for Re matched experiments. The piston velocity V in water is systematically varied to get the required Reynolds number. The stroke length L is kept constant at 100 mm for all experiments.

We compare the matched Re experiments only during the free shear motion of the ring, with the fully formed vortex ring as the starting point (time $t = 0$ in all the following plots as well as the subscript ‘0’ correspond to the end of the formation phase and the beginning of the free shear motion). We study the effect of matching the Reynolds number on vortex ring properties such as ring circulation, enstrophy, kinetic energy and peak vorticity. We plot these vortex ring properties in non-dimensional units. The vortex ring properties are normalised using their initial values, i.e., the values at the end of the formation stage. These normalised quantities are plotted against non-dimensional time. Time can be non-dimensionalised in two ways: (1) using an inertial time scale $t^* = t\Gamma_0/2\pi R_0^2$, and (2) using a viscous time scale $t^* = t\nu/2\pi R_0^2$, where, t is dimensional time, Γ_0 is initial circulation, R_0 is initial vortex ring radius and ν is kinematic viscosity of the solution. Since the vortex rings generated in the current experiments are at high Reynolds numbers ($Re \geq 1000$), the inertial force is more dominant over the viscous force. Hence, the inertial time scale is used for non-dimensionalising time. This method of non-dimensionalising time has been used earlier by Jha and Govardhan [22] and others [23, 24].

We demonstrate the expected behaviour of the circulation of the vortex ring at different Reynolds numbers using a schematic in Fig. 8a. A vortex ring with $Re \rightarrow \infty$ is an inviscid ring, and thus does not encounter any viscous effects. The ring is thus expected to propagate with an unchanged circulation for all time. On the other hand, for $Re \rightarrow 0$, the dominance of viscous forces would cause the vorticity to instantly diffuse, thereby reducing the circulation to zero. The circulation for all finite Re would lie in between these two limits, as shown in the figure.

We validate the above argument by comparing different Re experiments within each solution. Fig. 8 shows the normalised circulation as a function of non-dimensional time. We clearly observe the transition from an almost constant circulation at high Re to a rapid reduction in circulation as Re reduces. Hence, all the experiments in individual solutions, qualitatively demonstrate the Re based variation. Also, water shows the least variation in the curves of Γ/Γ_0 , while the PAMH 10 *ppm* solution shows the steepest reduction in Γ/Γ_0 at L100 V100. This indicates that, at L100 V100, the PAMH 10 *ppm* solution has the least Re amongst all the fluids and parameters considered.

We now compare the behaviour of polymer solution vortex rings with their respective limiting Re matched water vortex rings. Fig. 9 shows the normalised ring circulation as a function of non-dimensional time, with Figs. 9a and 9b showing this comparison for the PAMH 5 *ppm* (at V500) and PAMH 10 *ppm* (at V1000) solutions, respectively. We observe that Γ/Γ_0 for the PAMH 5 *ppm* solution lies in between the limiting water curves corresponding to Re_0 and Re_∞ . A similar behaviour is observed for the PAMH 10 *ppm* solution, but only until a point. Beyond $t^* \approx 0.8$, the circulation of the polymer ring reduces below the limiting curve of water corresponding to Re_0 . This indicates that the polymer solutions are initially within the limiting cases prescribed by water, but soon reduce to values below the lowest limit of Re .

Fig. 10 shows the variation of the normalised enstrophy for the vortex rings at matched Reynolds number, with Figs. 10a and 10b showing this variation for the PAMH 5 *ppm* and the PAMH 10 *ppm* solutions, respectively. We see from the plots that the enstrophy

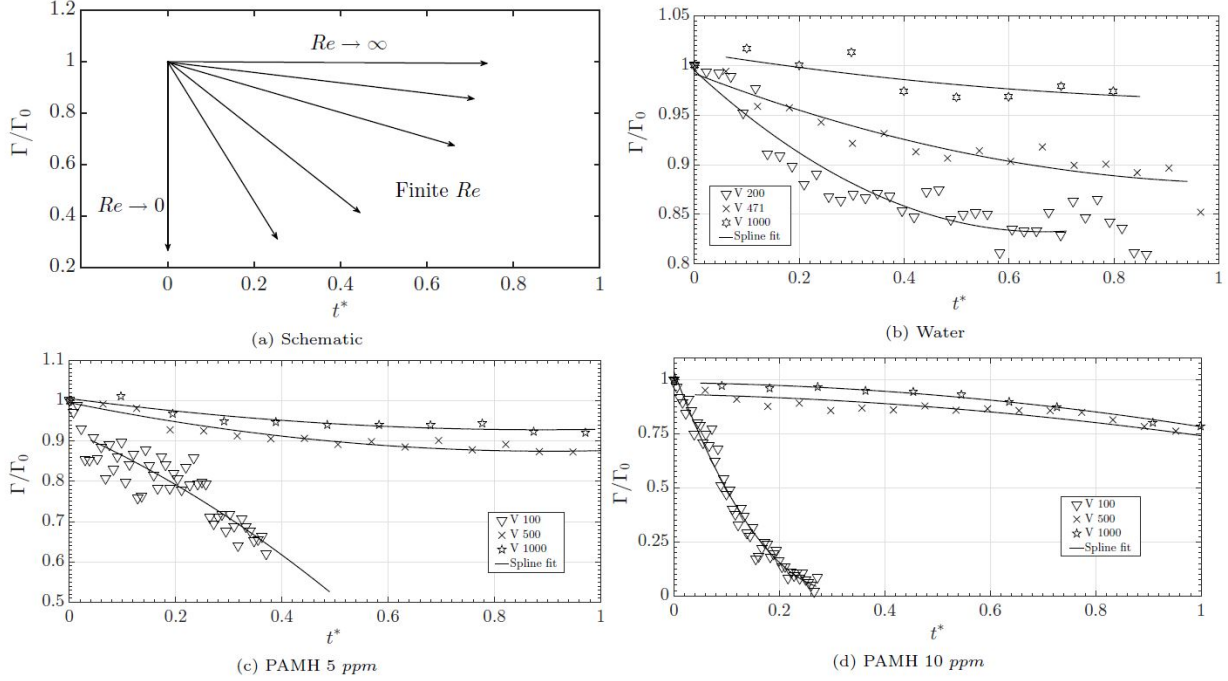


FIG. 8. Vortex ring circulation in non-dimensional co-ordinates at different Re . (a) shows the expected behaviour of circulation as Re is varied. (b), (c) and (d) show the normalised ring circulation for Water, PAMH 5 ppm and PAMH 10 ppm, respectively. Higher V yields a larger Re

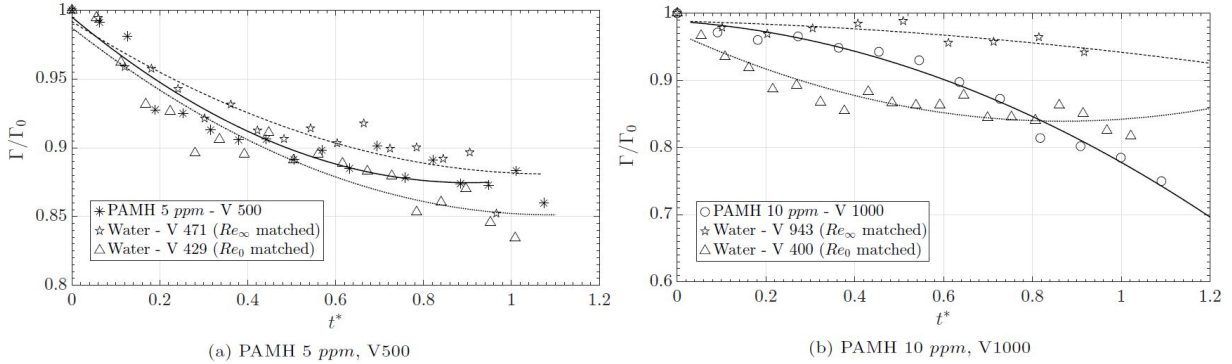


FIG. 9. Comparison of normalised vortex ring circulation for polymer solution experiments with its Re matched water experiments. Solid line represent spline fitted data for polymer solution. Dotted lines represent spline fitted data for corresponding water experiments.

of the PAMH vortex rings are always lesser than that of Water, falling even below the Re_0 matched Water vortex ring. This is a clear difference in the behaviour of Newtonian Water and the non-Newtonian PAMH solutions. Fig. 11 shows the variation of the normalised

peak vorticity (Fig. 11a) and the normalised area kinetic energy (Fig. 11b) as a function of non-dimensional time for the PAMH 10 *ppm* solution. We see, again, that the polymer solution shows a monotonic reduction in both these properties, and shows values considerably lower than the limiting values shown by Water.

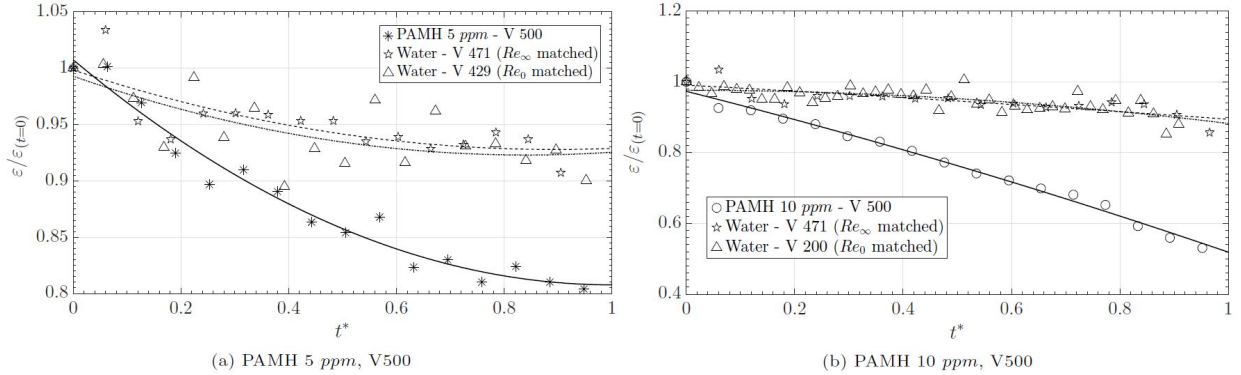


FIG. 10. Comparison of vortex ring enstrophy variation for polymer solution experiments with its Re matched water experiments. Solid line represent spline fitted data for polymer solution. Dotted lines represent spline fitted data for corresponding water experiments.

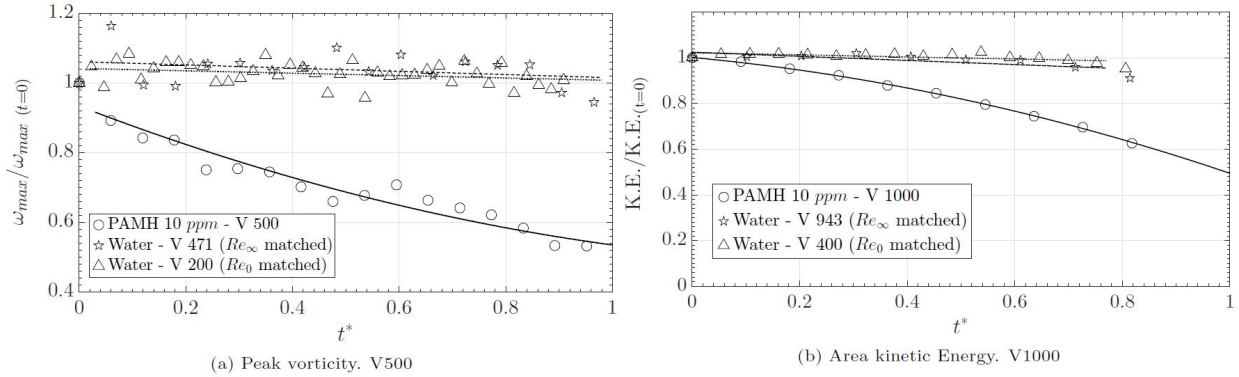


FIG. 11. Comparison of peak vorticity and kinetic energy for the PAMH 10 *ppm* experiment with its Re matched Water experiments. Solid line represent spline fitted data for polymer solution. Dotted lines represent spline fitted data for corresponding water experiments.

We now plot the vorticity distribution over one half of the vortex ring core for the Reynolds number matched experiments. Fig. 12 shows the vorticity distribution for Water at L100 V400 and the vorticity distribution for the PAMH 10 *ppm* solution at L100 V1000.

Piston parameters of the Water experiment correspond to the lowest Reynolds number Re_0 of the PAMH 10 *ppm* experiment. We see that, vorticity distributions are significantly shorter and broader for the polymer solutions even when compared to its low-limiting Re_0 Water counterpart. This causes the reduction in peak vorticity and enstrophy, as was observed in the constant impulse experiments as well.

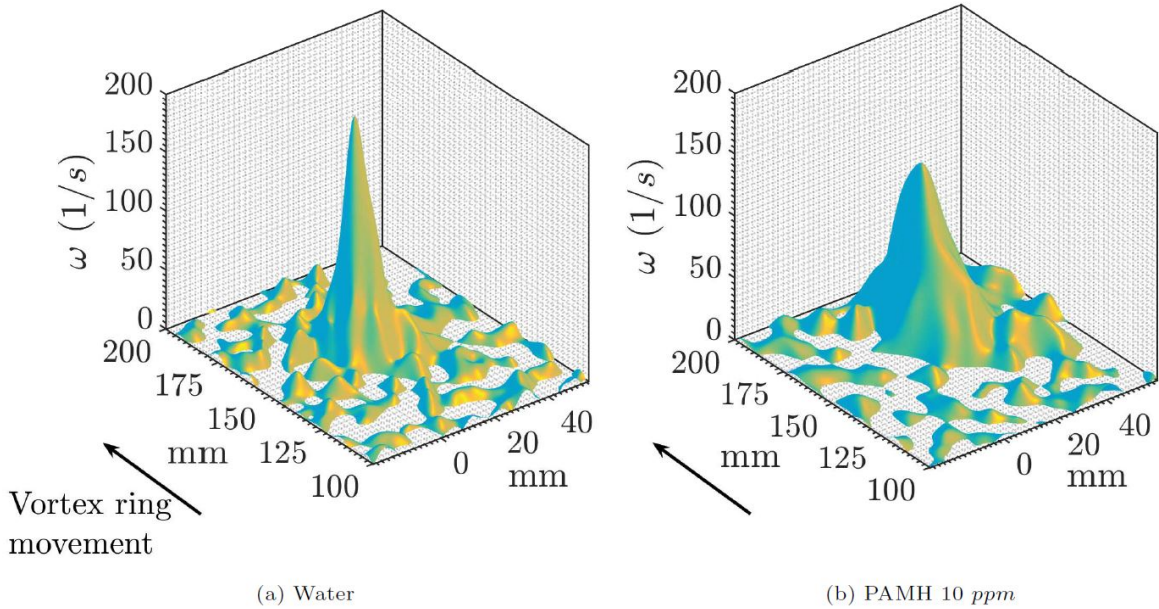


FIG. 12. Comparison of vorticity distribution over one half of the ring for PAMH 10 *ppm* - V 1000 experiment with its Re_0 matched water experiment - V400. Vorticity distribution over polymer ring is different even from its Re_0 matched experiment in water.

In this section, we have studied the effect of polymer solutions on the vortex ring by matching the Reynolds numbers for the Newtonian and the non-Newtonian rings. We find, similar to our observations at constant impulse, that the polymer solutions modify the vorticity distribution in the core of the vortex ring. This leads to lower values of the vortex ring properties, even when compared to the corresponding values at Re_0 (which is the lowest Re attainable by the polymer solutions) for Water. We conclude that matching the Reynolds numbers is insufficient to explain the behaviour of the non-Newtonian vortex rings.

VI. FORMATION NUMBER

The vortex ring forms when a slug of fluid pushed out of a nozzle rolls up. As the volume of the slug of fluid pushed out by the piston-cylinder mechanism increases, the vortex ring proportionately grows in size and circulation. Gharib et. al. showed [25], in a seminal work, that the vortex ring cannot grow indefinitely and that there exists a saturation of circulation for the vortex ring. This saturation of ring circulation occurs at $L \approx 4 \times D$. Beyond this value, any additional fluid ejected follows the ring as a trailing jet. This limiting non-dimensional stroke length is called the formation number.

The formation number has garnered attention due to its applications in underwater vehicles and bio-inspired propulsion [26]. Interestingly, this limiting L/D ratio is non-existent for vortex pairs, which are the 2-D Cartesian analogue of vortex rings [27–29]. Krueger et. al. [30] showed that the formation number changes in the presence of a background co-flow or counter-flow. Dabiri [31] has studied the effect of temporally varying nozzle exit diameter on vortex ring formation number. Gharib et. al. [6] demonstrated that cardiac health can be ascertained by measuring the efficiency of the heart in generating optimal vortex rings. This provides a necessary impetus to study the effect of non-Newtonian properties on the formation number of vortex rings

In this section, we conduct a set of experiments to study the effect of polymer solutions on the L/D ratio. We generate vortex rings at a single piston velocity ($V = 500 \text{ mm/s}$) and four different values of stroke lengths corresponding to L/D values of 2.88, 4.32, 5.76 and 7.2 for the PAMH 5 *ppm*, the PAMH 10 *ppm* and the PAMH 25 *ppm* solutions. For a Newtonian vortex ring, the trailing jet is absent at $L/D = 2.88$, a weak trailing jet is present at $L/D = 4.32$ and a strong trailing jet is present at $L/D = 5.76$ and $L/D = 7.2$.

We present the vorticity fields of vortex rings in PAMH solutions in Fig. 14 for the first three values of L/D ratio. The behaviour of the PAMH 5 *ppm* solution can be seen in Figs. 14a to 14c. The vorticity plots clearly show that the vortex ring is the only vortical structure at $L/D = 2.88$, and no trailing jet is present. At $L/D = 4.32$, the vortex ring is followed by a trailing jet. At $L/D = 5.76$, a strong trailing jet is visible behind the vortex ring. The

vorticity field of the PAMH 10 *ppm* solution is shown in Figs. 14d to 14f. We observe, as seen for the PAMH 5 *ppm* solution, that no trailing jet is present at $L/D = 2.88$, a weak trailing jet is present at $L/D = 4.32$ and a strong trailing jet is present at $L/D = 5.76$. The PAMH 25 *ppm* solution also shows a similar behaviour as the other two PAMH solutions, as seen in Figs. 14g to 14i. Figure 13 clearly shows that the primary vortex rings circulation saturates, although total circulation increases for $L/D \geq 4$.

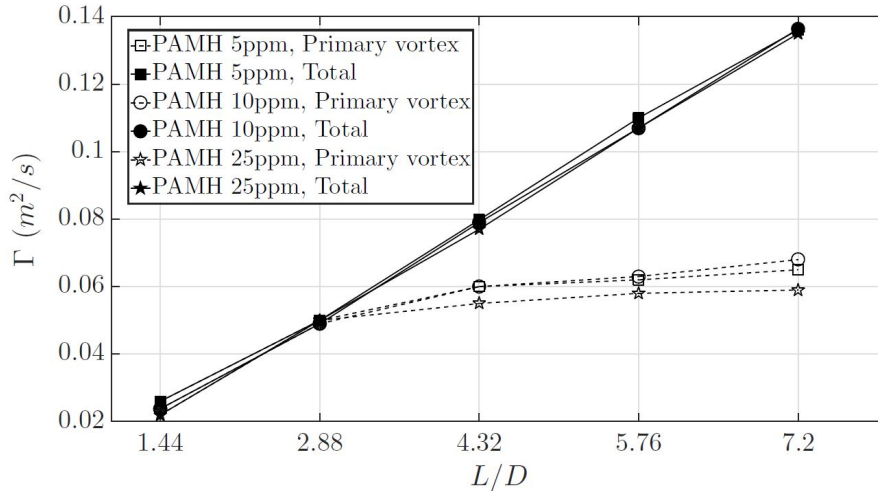


FIG. 13. Comparison of primary vortex ring circulation to total circulation

The vorticity plots seemingly show a trend of a weakening trailing jet as the polymer solution concentration increases. This is merely a consequence of plotting the vorticity fields for the three polymer solutions using a single set of vorticity levels.

It is clear from the vorticity maps that the trailing jet is dependent only on the value of the L/D and independent of the polymer concentration. Furthermore, the value of L/D at which the trailing jet begin to form closely correspond to that observed by Gharib et. al. [25]. We find that an isolated vortex ring is formed in the polymer solutions for $L/D \leq 4$, regardless of the concentration. Our observations also agree with those of Palacios-Morales [8], who noted a formation number of 4 in their vortex ring experiments in shear-thinning fluids.

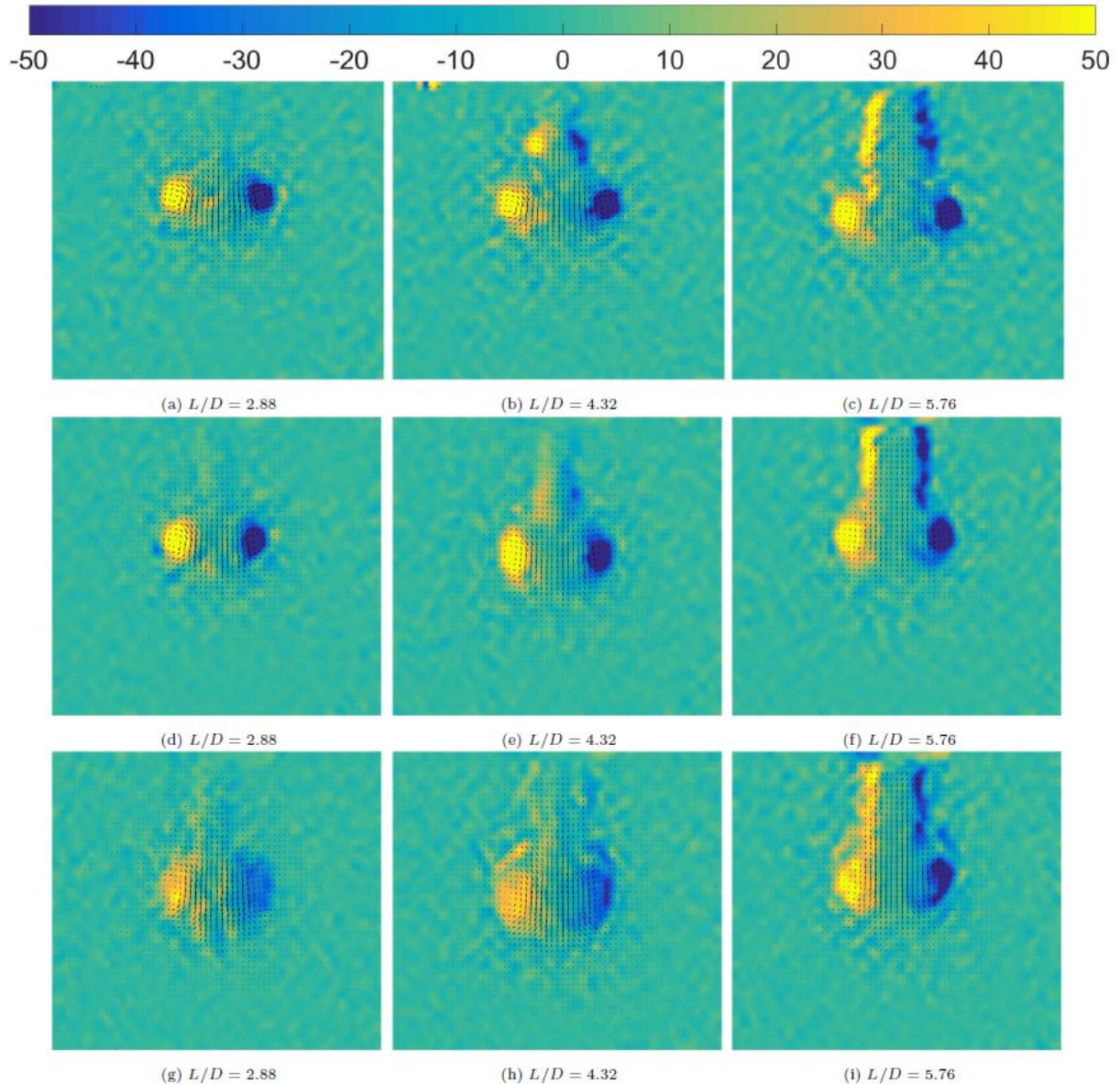


FIG. 14. Vorticity field for vortex rings generated in the PAMH solutions at different L/D ratios. (a) – (c) show vortex rings in the PAMH 5 *ppm* solution. (d) – (f) show vortex rings in the PAMH 10 *ppm* solution. (g) – (i) show vortex rings in the PAMH 25 *ppm* solution.

VII. ELASTIC EFFECTS

In this section, we report the behaviour of ‘ring reversal’ that was observed as the vortex rings came to a halt. The reduction in ring circulation causes the ring to continuously decelerate as it propagates forward. As the ring nears the end of its motion, elastic forces start to play a significant role. Palacios-Morales et. al. [10] have reported formation

of a ‘negative’ vortex ring ahead of the primary vortex ring. This ‘negative’ vortex ring halts the motion of the primary ring before causing it to disappear altogether. We perform planar laser induced fluorescence (PLIF) visualization to observe the behavior of the ring for PAMH 25 *ppm* solution.

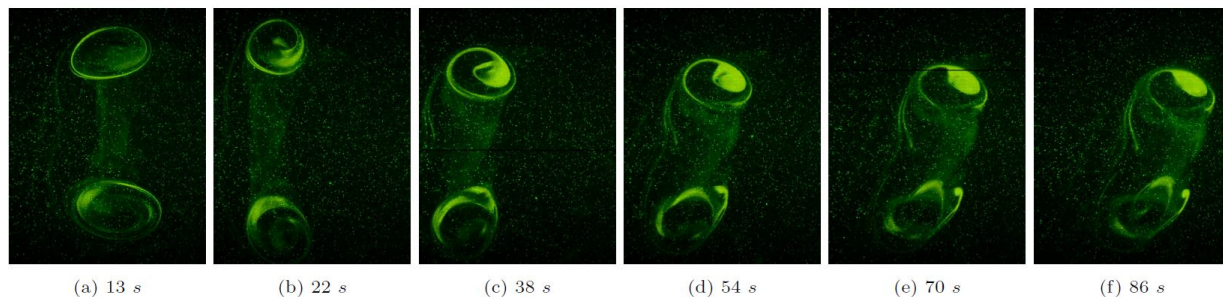


FIG. 15. Ring reversal in PAMH 25 *ppm* vortex rings at L100 V100. The forward motion of the ring is from right to left. The time steps mentioned correspond to the time elapsed since the formation of the vortex ring. The field of view is kept fixed, with the axial width corresponding to $\approx 1D$ ($4D - 5D$)

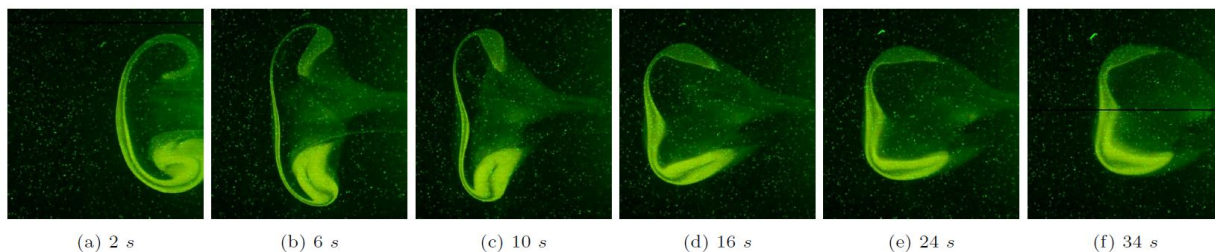


FIG. 16. Ring reversal in PAMH 25 *ppm* vortex rings at L50 V50. The forward motion of the ring is from right to left. The time steps mentioned correspond to the time elapsed since the formation of the vortex ring. The field of view is $\approx 1D$ ($1D - 2D$)

Fig. 15 shows the ‘ring reversal’ phenomenon in the PAMH 25 *ppm* solution at L100 V100. The sequence of images depict the change in direction of the ring’s motion. The forward motion of the ring ends in Fig. ???. The ring then starts ‘unrolling’ itself by moving in the opposite direction. This process is a slow one, as indicated by the timestamps. This ‘unrolling’ process is better observed at a lower impulse of L50 V50, as seen in Fig. 16. The forward motion of the vortex ring is quickly retarded, with the ring being pulled back

towards the nozzle. An interesting behaviour observed here is the tendency of the polymer solution to prevent the ring from rolling up - the ring is allowed to roll up to about half a turn (Fig. 16b). The ring is then forced to ‘unroll’ itself. The vorticity levels involved with negative vortex ring are very small and could not be accurately measured in our experiments.

The reduction in ring circulation and other vortex ring parameters have been attributed to the shear thinning viscosity profile [8, 9]. Palacios-Morales et. al. [10] show that elastic effects reinforce shear thinning effects with respect to the size and circulation of the vortex ring. The change in the vortex ring properties could be due to a combination of shear thinning effects and elastic effects with their individual contributions being unknown. It is thus difficult to decouple the effects of shear thinning and elasticity. The ‘ring reversal’ phenomenon is clearly an elastic phenomenon. The lack of ring inertia causes the ring to experience low shear rates, which corresponds to the zero shear plateau. The effect of shear thinning is thus non-existent.

VIII. CONCLUSION

We have conducted experiments on vortex rings in non-Newtonian polymer solutions. We have studied the effect of these polymer solutions on vortex ring properties such as ring circulation, enstrophy, kinetic energy, etc. We observe that the vortex ring parameters are considerably altered in the presence of the polymer solutions. Vortex ring properties such as the enstrophy and peak vorticity show significant differences when compared to Newtonian Water during the initial formation process of the ring. The kinetic energy and circulation are unaffected in this stage due to the conservation of the product of vorticity and area of the vorticity distribution in the polymer solutions. Once the vortex ring completes the formation process, all the vortex ring properties are severely affected by the polymer solutions.

The vortex rings generated in the polymer solutions were compared with Newtonian water in two ways: (1) by matching impulse generated by the piston, and (2) by matching the Reynolds number. The Reynolds number was matched at viscosities corresponding to the zero shear and the infinite shear plateaus polymer solution. The modification of the

vorticity distribution was evident in both these sets of experiments. It is interesting to note that the vorticity distribution of the polymer solution was significantly modified, even when compared to the vorticity distribution for Water at a Reynolds number corresponding to η_0 . We therefore suggest that it is this modification of the vorticity distribution that causes the changes in the vortex ring parameters observed. Some parameters, such as the ring circulation, show the effects of the modified vorticity distribution only after some time has elapsed, whereas most of the parameters, such as enstrophy and peak vorticity, show an immediate effect in their values.

We have studied the behaviour of vortex rings in polymer solutions with water-like viscosities and at high Reynolds numbers. These parameters are relevant to turbulent drag reduction, and the application of that phenomenon to industrial applications such as oil pipelines. We find that the behaviour of the vortex rings observed in this study is similar to that observed in previous work by Palacios-Morales [8] and Bentata et. al. [9], whose vortex rings were at significantly lower Reynolds numbers. We also demonstrated the ‘ring reversal’ phenomenon that is observed at low inertia situation of the vortex ring when the elastic effects are dominant. This behaviour qualitatively agrees with the ‘negative vortex ring’ that was observed by Palacios-Morales et. al. [10]. We also explored the effect of polymer solutions on the formation number of the vortex ring. We don’t observe any changes in the formation number for the vortex rings in polymer solution. The exact contribution of the shear thinning effects and viscoelastic effects on the vortex ring properties observed in this study is still not known. Experiments which can decouple these effects, particularly at high Reynolds numbers would help in understanding this interaction of dissolved polymers in solution with canonical vortex structures such as the vortex ring. Such experiments might also help in better understanding the complicated phenomenon of turbulent polymer drag reduction.

[1] P. Linden, The interaction of a vortex ring with a sharp density interface: a model for turbulent entrainment, *Journal of Fluid Mechanics* 60 (3) (1973) 467–480.

- [2] S. Advait, K. Manu, A. Tinaikar, U. K. Chetia, S. Basu, Interaction of vortex ring with a stratified finite thickness interface, *Physics of Fluids* 29 (9) (2017) 093602.
- [3] R. M. Kerr, Numerical generation of a vortex ring cascade in quantum turbulence, arXiv preprint arXiv:1006.3911.
- [4] D. Liepmann, M. Gharib, The role of streamwise vorticity in the near-field entrainment of round jets, *Journal of Fluid Mechanics* 245 (1992) 643–668.
- [5] K. Sreenivas, A. K. Prasad, Vortex-dynamics model for entrainment in jets and plumes, *Physics of Fluids* 12 (8) (2000) 2101–2107.
- [6] M. Gharib, E. Rambod, A. Kheradvar, D. J. Sahn, J. O. Dabiri, Optimal vortex formation as an index of cardiac health, *Proceedings of the National Academy of Sciences* 103 (16) (2006) 6305–6308.
- [7] D. An, A. Warning, K. G. Yancey, C.-T. Chang, V. R. Kern, A. K. Datta, P. H. Steen, D. Luo, M. Ma, Mass production of shaped particles through vortex ring freezing, *Nature communications* 7 (2016) 12401.
- [8] C. Palacios-Morales, R. Zenit, The formation of vortex rings in shear-thinning liquids, *Journal of Non-Newtonian Fluid Mechanics* 194 (2013) 1–13.
- [9] O. Bentata, D. Anne-Archard, P. Brancher, Experimental study of low inertia vortex rings in shear-thinning fluids, *Physics of Fluids* 30 (11) (2018) 113103.
- [10] C. Palacios-Morales, C. Barbosa, F. Solorio, R. Zenit, Negative vortices: The formation of vortex rings with reversed rotation in viscoelastic liquids, *Physics of Fluids* 27 (5) (2015) 051703.
- [11] J. Olsthoorn, M. Stastna, D. Steinmoeller, On the dynamics of vortex-wall interaction in low viscosity shear thinning fluids, *Physics of Fluids* 26 (1) (2014) 013101.
- [12] R. J. Adrian, Twenty years of particle image velocimetry, *Experiments in fluids* 39 (2) (2005) 159–169.
- [13] R. J. Adrian, J. Westerweel, *Particle image velocimetry*, no. 30, Cambridge University Press, 2011.
- [14] A. K. Prasad, Particle image velocimetry, *Current Science* 79 (1) (2000) 51–60.
- [15] M. Raffel, C. E. Willert, F. Scarano, C. J. Kähler, S. T. Wereley, J. Kompenhans, *Particle image velocimetry: a practical guide*, Springer, 2018.
- [16] J. Westerweel, *Fundamentals of digital particle image velocimetry*, Measurement science and

- technology 8 (12) (1997) 1379.
- [17] S. Hegde, Experimental investigation of vortex ring evolution and wall interaction in polymer solution, Master's thesis, JNCASR, India (2018).
 - [18] S. Srinivas, V. Kumaran, Effect of viscoelasticity on the soft-wall transition and turbulence in a microchannel, *Journal of Fluid Mechanics* 812 (2017) 1076–1118.
 - [19] Y. Zhang, S. J. Muller, Unsteady sedimentation of a sphere in wormlike micellar fluids, *Physical Review Fluids* 3 (4) (2018) 043301.
 - [20] A. Weigand, M. Gharib, On the evolution of laminar vortex rings, *Experiments in Fluids* 22 (6) (1997) 447.
 - [21] K. Shariff, A. Leonard, Vortex rings, *Annual Review of Fluid Mechanics* 24 (1) (1992) 235–279.
 - [22] N. K. Jha, R. Govardhan, Interaction of a vortex ring with a single bubble: bubble and vorticity dynamics, *Journal of Fluid Mechanics* 773 (2015) 460–497.
 - [23] D. J. Asselin, C. Williamson, Influence of a wall on the three-dimensional dynamics of a vortex pair, *Journal of Fluid Mechanics* 817 (2017) 339–373.
 - [24] D. Harris, C. Williamson, Instability of secondary vortices generated by a vortex pair in ground effect, *Journal of Fluid Mechanics* 700 (2012) 148–186.
 - [25] M. Gharib, E. Rambod, K. Shariff, A universal time scale for vortex ring formation, *Journal of Fluid Mechanics* 360 (1998) 121–140.
 - [26] J. O. Dabiri, Optimal vortex formation as a unifying principle in biological propulsion, *Annual review of fluid mechanics* 41 (2009) 17–33.
 - [27] L. Gao, S. Yu, Formation of leading vortex pair in two-dimensional starting jets, *AIAA Journal* 54 (1) (2016) 1364–1369.
 - [28] Y. Afanasyev, Formation of vortex dipoles, *Physics of fluids* 18 (3) (2006) 037103.
 - [29] G. Pedrizzetti, Vortex formation out of two-dimensional orifices, *Journal of Fluid Mechanics* 655 (2010) 198–216.
 - [30] P. S. Krueger, J. O. Dabiri, M. Gharib, The formation number of vortex rings formed in uniform background co-flow, *Journal of Fluid Mechanics* 556 (2006) 147–166.
 - [31] J. O. Dabiri, M. Gharib, Starting flow through nozzles with temporally variable exit diameter, *Journal of Fluid Mechanics* 538 (2005) 111–136.